Published in final edited form as:
J Hepatol. 2012 August ; 57(2): 359–365. doi:10.1016/j.jhep.2012.03.025.

Mouse organic solute transporter alpha deficiency alters FGF15 expression and bile acid metabolism

Tian Lan[1], **Anuradha Rao**[1], **Jamie Haywood**[1], **Nancy D. Kock**[2], and **Paul A. Dawson**[1,2,*]

[1]Department of Internal Medicine, Wake Forest University School of Medicine, Medical Center Blvd., Winston-Salem, NC 27157, USA

[2]Department of Pathology, Wake Forest University School of Medicine, Medical Center Blvd., Winston-Salem, NC 27157, USA

Abstract

Background & Aims—Blocking intestinal bile acid (BA) absorption by inhibiting or inactivating the apical sodium-dependent BA transporter (Asbt) classically induces hepatic BA synthesis. In contrast, blocking intestinal BA absorption by inactivating the basolateral BA transporter, organic solute transporter alpha–beta (Ostα–Ostβ) is associated with an altered homeostatic response and decreased hepatic BA synthesis. The aim of this study was to determine the mechanisms underlying this phenotype, including the role of the farnesoid X receptor (FXR) and fibroblast growth factor 15 (FGF15).

Methods—BA and cholesterol metabolism, intestinal phenotype, expression of genes important for BA metabolism, and intestinal FGF15 expression were examined in wild type, *Osta*$^{-/-}$, *Fxr*$^{-/-}$, and *Osta*$^{-/-}$*Fxr*$^{-/-}$ mice.

Results—Inactivation of *Osta* was associated with decreases in hepatic cholesterol 7α-hydroxylase (Cyp7a1) expression, BA pool size, and intestinal cholesterol absorption. *Osta*$^{-/-}$ mice exhibited significant small intestinal changes, including altered ileal villus morphology, and increases in intestinal length and mass. Total ileal FGF15 expression was elevated almost 20-fold in *Osta*$^{-/-}$ mice as a result of increased villus epithelial cell number and ileocyte FGF15 protein expression. *Osta*$^{-/-}$*Fxr*$^{-/-}$ mice exhibited decreased ileal FGF15 expression, restoration of intestinal cholesterol absorption, and increases in hepatic Cyp7a1 expression, fecal BA excretion, and BA pool size. FXR deficiency did not reverse the intestinal morphological changes or compensatory decrease for ileal Asbt expression in *Osta*$^{-/-}$ mice.

Conclusions—These results indicate that signaling via FXR is required for the paradoxical repression of hepatic BA synthesis but not the complex intestinal adaptive changes in *Osta*$^{-/-}$ mice.

Keywords

Bile acids; Enterohepatic circulation; Transporters; Cholesterol; Cyp7a1; FXR

Corresponding author. Address: Department of Internal Medicine, Wake Forest University School of Medicine, Medical Center Blvd., Winston-Salem, NC 27157, USA. Tel.: +1 (336) 716 4633; fax: +1 (336) 716 6276. pdawson@wakehealth.edu (P.A. Dawson).

Conflict of interest

The authors who have taken part in this study declared that they do not have anything to disclose regarding funding or conflict of interest with respect to this manuscript.

Supplementary data

Supplementary data associated with this article can be found, in the online version, at http://dx.doi.org/10.1016/j.jhep.2012.03.025.

Introduction

Regulation of hepatic expression of Cyp7a1, the rate-limiting enzyme for the classical BA biosynthetic pathway, is complex and integrates responses to hormones, cytokines, growth factors, oxysterols, BA, xenobiotics, and diurnal rhythm [1]. It is well established that the nuclear receptor FXR is essential for negative feedback regulation of *Cyp7a1* by BA [2,3]. However, a critical role for gut-liver signaling via the endocrine polypeptide hormone FGF15 (human ortholog: FGF19) has only recently been appreciated [4,5]. In that pathway, BA act as ligands for FXR in ileal enterocytes to induce synthesis of FGF15. After its release into the circulation, FGF15 acts on hepatocytes through its cell surface receptor, a complex of β-Klotho protein and fibroblast growth factor receptor-4 (FGFR4), to repress *Cyp7a1* expression and BA synthesis [4-6].

After their hepatic synthesis and secretion into the small intestine, BA are efficiently reabsorbed by active transport in the ileum and transported back to the liver [7]. In the ileum, BA are transported across the apical brush border membrane via the Asbt (gene symbol *Slc10a2*) [7], whereas the heteromeric transporter Ostα–Ostβ (gene symbols: *Osta, Slc51a1*; *Ostb, Slc51a1bp*) is responsible for basolateral membrane transport [8-10]. Resection of terminal ileum, ileal disease, or inactivation of Asbt in humans or mice interrupts the enterohepatic circulation of BA and results in increased fecal levels of BA, induction of hepatic *Cyp7a1* expression and BA synthesis, and partial depletion of the BA pool [11-14]. Although ileal BA transport is also impaired in $Osta^{-/-}$ mice, these animals do not exhibit the classical response to intestinal BA malabsorption [9,10]. The BA phenotype of $Osta^{-/-}$ mice is more similar to that observed in $Asbt^{-/-}$ mice treated with an FXR agonist or an FGF15-expressing adenovirus [13]. Those observations provide a possible explanation for the phenotype in $Osta^{-/-}$ mice whereby blocking basolateral export causes BA to accumulate in ileal enterocytes, leading to persistent activation of FXR, increased FGF15 expression, and the unexpected repression of hepatic BA synthesis [9].

Portions of this work were presented at the 2010 Annual Meeting of the American Association for the Study of Liver Disease and the 21st International Bile Acid Meeting entitled “Falk Symposium 175: Bile Acids as Metabolic Integrators and Therapeutics” and published in abstract and meeting proceedings form [15,16].

Materials and methods

Animals, diets and treatment studies

The Institutional Animal Care and Use Committee approved these experiments. $Fxr^{-/-}$ mice (Jackson Laboratory Stock#: 004144, Strain: B6;129X(FVB)-Nr1h4^{tm1Gonz}/J) were bred with $Osta^{-/-}$ mice (C57BL/6J-129/SvEv) [9] to generate the required genotypes. Unless indicated, the mice were fed *ad libitum* standard rodent chow. In selected studies, mice were fed a basal diet [14] or a basal diet supplemented with 0.2% (w/w) cholic acid (CA) (Sigma–Aldrich). For analysis of ileal FGF15 protein expression, groups of non-fasted WT mice were treated with a single oral gavage of 100 mg/kg body weight of the FXR agonist, GW4064 (a gift from Dr. Timothy Willson, GlaxoSmithKline), or vehicle (Polyethylene glycol 400/Tween 80; 4:1, v/v). FGF15 protein expression was also examined in ileal extracts from WT and $Asbt^{-/-}$ mice maintained on the basal diet [14] and WT and $Fgf15^{-/-}$ mice (a gift from Dr. Steve Kliewer, University of Texas Southwestern Medical Center) [17].

Histology

The small intestine was subdivided into five equal length segments and processed for histology. Villus height and width, crypt depth, and muscle thickness were measured for all

intestinal segments in at least 20 well-oriented, full-length villus units per mouse. Quantitative analyses were performed by AxioVision analysis of digitally acquired images.

BA and lipid measurements

Feces were collected to measure total BA content by enzymatic assay and neutral sterol content by gas–liquid chromatography. Intestinal cholesterol absorption was measured using the fecal dual-isotope ratio method; BA pool size was determined as the BA content of small intestine, liver, and gallbladder [14]. BA composition was determined by HPLC [18] and used to calculate the pool hydrophobicity [19]. Plasma BA were determined by enzymatic assay (Bio-Quant Inc.) and found to be similar between the different groups (WT, 52 ± 4 μM; *Fxr*$^{-/-}$, 67 ± 10 μM; *Osta*$^{-/-}$, 52 ± 7 μM; *Osta*$^{-/-}$*Fxr*$^{-/-}$, 66 ± 13 μM; n = 3–5 male mice per group). To measure ileal-associated BA, the small intestine was divided into five equal segments, flushed with PBS, and ground under liquid nitrogen using a mortar and a pestle. Aliquots of ileal tissue were then used to isolate RNA or extracted to measure tissue-associated BA [20]. Plasma and hepatic levels of total cholesterol, free cholesterol, and triglyceride were determined by enzymatic assay (Roche Applied Science) [14].

Measurements of nucleic acid content and mRNA expression

Small intestinal DNA and RNA content was measured using modifications [21] of the diphenylamine and orcinol colorimetric methods, respectively. Total RNA was extracted from frozen tissue using TRIzol Reagent (Invitrogen). Real time PCR analysis was performed as described [9]; values are means of triplicate determinations and expression was normalized using cyclophilin. The primer sequences used are provided (Supplementary Table 1). Whole intestinal segment mRNA expression was calculated by normalizing to total RNA content. Unless otherwise indicated, expression levels were plotted relative to WT mice.

Measurements of protein expression

A rabbit polyclonal antibody was raised against a glutathione-S-transferase fusion protein (Amersham Biosciences) encompassing amino acids 171–218 of mouse FGF15, and purified by affinity chromatography using the same antigen coupled to agarose beads (Amino-Link Immobilization Kit; Pierce). Sources of other antibodies were as follows: anti-mouse Asbt [14], anti-mouse apoA-I [22], anti-β-actin (Sigma–Aldrich, A5441), HRP-conjugated anti-rabbit (Sigma–Aldrich, A9169; or Cell Signaling, 7074), HRP-conjugated anti-mouse (GE Healthcare, NXA931). Small intestinal extracts were prepared, subjected to SDS–PAGE using 8% or 4–12% gradient (Bis-Tris Midi Gel, Invitrogen) polyacrylamide gels, and analyzed by immunoblotting [9]. Blots were stripped and reprobed with antibody to β-actin to normalize for protein load. Protein expression was quantified by densitometry using a Microtek ScanMaker i900 and FujiFilm Multiguage 3 software, and expression data was normalized to levels of the β-actin loading control.

Statistical analyses

Mean values ± SE are shown unless otherwise indicated. The data were evaluated for statistically significant differences using the two-tailed Student's *t* test or by ANOVA (Tukey–Kramer honestly significant difference) (Statview; Mountain View, CA). Differences were considered statistically significant at $p < 0.05$ and are indicated by different lowercase letters in the figures.

Results

BA and cholesterol metabolism

Deletion of *FXR* in *Osta*$^{-/-}$ mice resulted in a phenotype typically observed following a block in intestinal BA absorption. Fecal BA excretion was similar between *Osta*$^{-/-}$ and WT mice, and induced by 2 to 3-fold in *Osta*$^{-/-}$*Fxr*$^{-/-}$ mice (Fig. 1A; Supplementary Fig. 1A). The BA pool size was increased approximately 1.8-fold in *Osta*$^{-/-}$*Fxr*$^{-/-}$ *vs. Osta*$^{-/-}$ mice (Fig. 1B; Supplementary Fig. 1B), but did not reach the levels in WT or *Fxr*$^{-/-}$ due to increased fecal BA loss. The BA pool also became enriched in taurocholate and more hydrophobic in *Osta*$^{-/-}$*Fxr*$^{-/-}$ *vs. Osta*$^{-/-}$ mice, as reflected by an increase in the hydrophobicity index. The TβMC:TC ratio was also increased (*Osta*$^{-/-}$ *vs. Osta*$^{-/-}$*Fxr*$^{-/-}$; males: 0.42 ± 0.07 *vs.* 1.48 ± 0.20; females 0.35 ± 0.03 *vs.* 0.70 ± 0.10) (Fig. 1B and C; Supplementary Fig. 1B and C), suggesting a derepression of hepatic BA synthesis via the Cyp7a1 pathway.

Since intestinal cholesterol absorption is greatly affected by luminal BA concentration and BA pool hydrophobicity [14,23], fecal neutral sterol excretion and cholesterol absorption were also examined in the different genotypes. Fecal neutral sterol excretion was increased in *Osta*$^{-/-}$ mice, reflecting a dramatic reduction in intestinal cholesterol absorption (Fig. 1D and E; Supplementary Fig. 1D). This phenotype was largely reversed by introducing FXR deficiency (Fig. 1E; Supplementary Fig. 1D) or by feeding a diet containing a more hydrophobic BA (0.2% CA) (Fig. 1F; Supplementary Fig. 1E). Plasma cholesterol and triglyceride levels were not significantly altered in male *Osta*$^{-/-}$ mice; FXR deficiency tended to increase plasma cholesterol and triglyc-eride levels, as observed previously [24], and this effect was maintained in the *Osta*$^{-/-}$ background (Supplementary material and methods). Hepatic cholesteryl ester (CE) content was increased approximately 2.5-fold in *Osta*$^{-/-}$ mice (Fig. 1G), in agreement with the predicted decrease in hepatic conversion of cholesterol to BA. In contrast to *Asbt*$^{-/-}$ mice [14], hepatic cholesteryl ester content was not decreased in *Osta*$^{-/-}$*Fxr*$^{-/-}$ mice. Hepatic triglyceride levels tended to be higher in *Osta*$^{-/-}$ but not *Osta*$^{-/-}$*Fxr*$^{-/-}$ mice (Fig. 1H).

Morphology of the small intestine

Osta$^{-/-}$ mice were indistinguishable from adult WT or *Fxr*$^{-/-}$ mice with regard to body weight or liver weight (data not shown), however, there were significant small intestinal changes that were not reversed by inactivation of FXR (Fig. 2). The small intestine was significantly heavier in both *Osta*$^{-/-}$ and *Osta*$^{-/-}$*Fxr*$^{-/-}$ mice *vs.* WT mice. Since Ostα–Ostβ exhibits a gradient of expression along the small intestine length with the highest levels in ileum, the segmental distribution for the intestinal mass was also examined. In agreement with this pattern of expression, significant mass changes were evident in the distal small intestine of *Osta*$^{-/-}$ mice, where intestinal weight per unit length was increased approximately 66% (Supplementary Fig. 2A). Similar changes were observed in female mice (data not shown). The ileal content of DNA and RNA was increased approximately 2-fold in *Osta*$^{-/-}$ mice as compared with WT mice (Supplementary Fig. 2B and C), reflecting an increase in cell number. These small intestinal changes persisted in *Osta*$^{-/-}$*Fxr*$^{-/-}$ mice (Supplementary Fig. 2).

In *Osta*$^{-/-}$ and *Osta*$^{-/-}$*Fxr*$^{-/-}$ mice, ileal but not jejunal morphology was significantly altered (Fig. 2C and D), where the villi were blunted and thickened (fused), with evidence of enterocyte dysplasia and occasionally dilated lacteals. Morphometric measurements were performed using histological sections of small intestine from the four genotypes. Muscle thickness was unchanged, but villi in ileum of *Osta*$^{-/-}$ and *Osta*$^{-/-}$Fxr$^{-/-}$ mice were shorter and wider, with deeper crypts (Supplementary Fig. 3). There was a slight increase in

lymphocytes and plasma cells in the lamina propria of *Osta*$^{-/-}$ mice (Fig. 2C), but no associated increases in expression of selected pro-inflammatory genes or genes involved in ER stress (data not shown).

Hepatic and intestinal gene expression

Hepatic *Cyp7a1* mRNA expression was decreased by 74% in *Osta*$^{-/-}$ mice and increased 2-fold in *Osta*$^{-/-}$*Fxr*$^{-/-}$ mice *vs*. WT mice (Table 1). Effects of *Osta* inactivation were greater for hepatic *Cyp7a1* than *Cyp8b1* mRNA expression, consistent with previous findings demonstrating that Cyp7a1 is more strongly regulated by FGF15 signaling [25]. Analysis of the hepatic mRNA expression of other genes involved in hepatic bile acid or cholesterol metabolism revealed an increase in FXRα3,4 isoforms in *Osta*$^{-/-}$ mice. However, there were few other significant changes with the exception of decreases in MRP2 and SR-BI, which were not reversed by inactivation of FXR (Table 1). The decrease in hepatic Cyp7a1 expression was predicted to be secondary to an induction of ileal FGF15 expression [9]. Measurements revealed no significant change in the ileocyte *FGF15* mRNA (normalized to the housekeeping gene cyclophilin) but total ileal *FGF15* mRNA expression (normalized for increased ileal RNA content secondary to intestinal morphological changes) was increased approximately 2-fold in *Osta*$^{-/-}$ mice (Fig. 3A). The relatively small change in total *FGF15* mRNA levels prompted us to examine FGF15 protein expression (Fig. 3B and C). As a control, FGF15 protein expression was determined under conditions known to alter ileal *FGF15* mRNA expression [4,13]. As predicted, ileal FGF15 protein levels were increased in GW4064-treated WT mice, reduced in *Asbt*$^{-/-}$ mice, and undetectable in *Fgf15*$^{-/-}$ *vs*. WT mice (Fig. 3B). Remarkably, immunoblotting revealed a more than 10-fold increase for ileal FGF15 protein expression in *Osta*$^{-/-}$ mice (Fig. 3C). There was no accompanying change in the intestinal gradient for FGF15 expression in Ostα$^{-/-}$ mice, nor does this increase appear to be due to a non-specific protein retention or delayed protein secretion by the ileal enterocytes, since ileal apo A-I protein levels were not increased (Supplementary Fig. 4). Accounting for the elevated ileal protein content of *Osta*$^{-/-}$ *vs*. WT mice, total ileal FGF15 protein is increased almost 20-fold (Fig. 3C). The mRNA and protein expressions of FGF15 were both dramatically reduced in ileum of *Fxr*$^{-/-}$ and *Osta*$^{-/-}$*Fxr*$^{-/-}$ mice.

Ileal gene expression and BA accumulation

The surprising finding that ileocyte *FGF15* mRNA expression (normalized to expression of the housekeeping gene cyclophilin) was not increased in *Osta*$^{-/-}$ mice (Fig. 3A) prompted an examination of other FXR target genes. Ileal expression of Ibabp, Ostβ, PXR, Shp, and sodium-sulfate co-transporter (*Slc13a1*) was found to be reduced rather then increased in *Osta*$^{-/-}$ mice (Table 2). A variety of mechanisms could modulate ileal expression of FXR target genes in *Osta*$^{-/-}$ mice including: (1) altered FXR expression or activity, (2) decreased BA uptake by the ileal enterocyte, and (3) altered BA pool size or composition. Measurements of ileal *FXR* mRNA levels revealed significant decreases of individual FXR isoform and total FXR expression (Table 2). Another possible adaptation in *Osta*$^{-/-}$ mice is a decreased BA uptake. As shown in Fig. 4, ileal Asbt protein expression is reduced almost 80% in both *Osta*$^{-/-}$ and *Osta*$^{-/-}$*Fxr*$^{-/-}$ *vs*. WT mice. The BA pool's decreased size and enrichment in muricholic acid, a poor FXR ligand [26], may also contribute to the reduced expression of FXR target genes in *Osta*$^{-/-}$ mice. To examine this possibility, mice were fed a diet containing a 0.2% CA, an active FXR ligand, and ileal BA accumulation and gene expression were measured (Fig. 4C–F). Expression of ileal FXR target genes *Ibabp* and *FGF15* was reduced in *Osta*$^{-/-}$ mice *vs*. WT mice (Fig. 4E and F). Their reduced expression correlated with a decreased ileal BA content, which is likely to be secondary to reduced Asbt expression. Inactivation of *Osta* was also associated with reduced expression of other non-FXR target genes such as *ABCA1, ABCG5, HNF4a*, and *NPC1L1*. Interestingly, their expression was not restored to WT levels in *Osta*$^{-/-}$*Fxr*$^{-/-}$ mice.

Discussion

The major finding of this study is that FXR is required for the unanticipated changes in BA homeostasis but not the complex intestinal morphological changes observed in *Osta*$^{-/-}$ mice. Moreover the original model [9], which proposed that the unexpected repression of hepatic BA synthesis in *Osta*$^{-/-}$ mice resulted from ileal enterocyte BA accumulation and increased expression of FXR-target genes, must be revised. The phenotypic changes in *Osta*$^{-/-}$ mice are summarized in Table 3.

Analysis of *Osta*$^{-/-}$ mice revealed significant histological and morphometric changes in ileum, including villi that were consistently blunted and fused. These changes, which are typically associated with damage and subsequent healing, have not been reported for patients or mouse models with primary BA malabsorption, a defect in apical brush border membrane transport [14,27]. The adult *Osta*$^{-/-}$ mice do not exhibit symptoms of persistent on-going intestinal injury, as indicated by the absence of elevated inflammatory gene expression, bleeding, or diarrhea. However, newborn *Osta*$^{-/-}$ mice exhibit a postnatal growth deficiency [9,10], and this may coincide with the onset of injury or initiation of the adaptive response. Although the underlying mechanisms and role of BA in this process remain to be determined, the finding of a similar intestinal phenotype in *Osta*$^{-/-}$ and *Osta*$^{-/-}$*Fxr*$^{-/-}$ mice argues against a role of the FXR-FGF15 pathway.

The classical physiological response to interruption of the enterohepatic circulation is increased hepatic BA synthesis [13,14,28,29]. However, despite evidence of a block in intestinal BA absorption, *Osta*$^{-/-}$ mice have decreased hepatic Cyp7a1 expression and no increase in fecal BA excretion [9,10]. In order to further understand how inhibiting BA transport at the enterocyte apical *vs*. basolateral membrane produces such different hepatic responses, the contribution of the FXR-FGF15 pathway to this unexpected BA phenotype was investigated. Inactivation of FXR in *Osta*$^{-/-}$ mice decreased ileal FGF15 expression and *Osta*$^{-/-}$Fxr$^{-/-}$ mice largely recapitulated the classical BA malabsorption phenotype. In *Osta*$^{-/-}$*Fxr*$^{-/-}$ mice, the BA composition and the intestinal cholesterol absorption were restored to near WT levels, consistent with the superior ability of TC *vs*. TβMC to solubilize and deliver cholesterol to the intestinal epithelial cells [23]. The decreased intestinal cholesterol absorption in *Osta*$^{-/-}$ mice is balanced by reduced cholesterol demand for hepatic BA synthesis. As a result, hepatic cholesteryl ester levels are only mildly elevated and plasma cholesterol levels are unchanged in male *Osta*$^{-/-}$ mice. Interestingly, there were few other significant changes in the hepatic expression of genes involved in BA homeostasis in *Osta*$^{-/-}$ mice and these changes were not reversed by inactivation of FXR.

Another goal of this study was to identify additional protective mechanisms engaged in *Osta*$^{-/-}$ mice. Surprisingly, inactivation of *Osta* did not lead to ileal BA accumulation. The mechanisms responsible for the decreased BA accumulation and reduced expression of FXR target genes appear to be multi-fold and may include decreased ileal expression of FXR [30]. Changes in BA pool size and composition are unlikely to be major factors since expression of FXR target genes remained lower in *Osta*$^{-/-}$ mice fed a CA-containing diet. However, a major protective mechanism in *Osta*$^{-/-}$ mice appears to be reduced Asbt expression [30]. This response does not require FXR, nor does it appear to be due to FGF15 acting in a paracrine fashion [31], since Asbt expression remains suppressed in the *Osta*$^{-/-}$*Fxr*$^{-/-}$ mice where FGF15 expression is markedly reduced. Another surprising finding was that the increase in ileal FGF15 production in *Osta*$^{-/-}$ mice results from a combination of elevated FGF15 protein expression and increased number of FGF15-expressing enterocytes.

These results affirm the critical role for Ostα–Ostβ in BA absorption and metabolism and the importance of FGF15 in regulating hepatic BA synthesis. The significance of these findings with regard to human hepatic or gastrointestinal disease is unknown. However, dysregulation of FGF19 production and hepatic BA overproduction have been implicated in the etiology of idiopathic BA malabsorption [32] and a similar phenotype of decreased BA absorption coupled with an inability of the liver to synthesize additional BA was previously described for gallstone patients [33].

Supplementary Material

Refer to Web version on PubMed Central for supplementary material.

Acknowledgments

Financial support

This project was supported by the NIH (DK047987) and an American Heart Association Mid-Atlantic Affiliate Grant-in-aid (to P.A.D.). A.R. was supported by the NIH (F32 DK079576).

The underlying research reported in this study was funded by the NIH Institutes of Health.

References

1. Chiang JY. Bile acids: regulation of synthesis. J Lipid Res. 2009; 50:1955–1966. [PubMed: 19346330]
2. Lu TT, Makishima M, Repa JJ, Schoonjans K, Kerr TA, Auwerx J, et al. Molecular basis for feedback regulation of bile acid synthesis by nuclear receptors. Mol Cell. 2000; 6:507–515. [PubMed: 11030331]
3. Goodwin B, Jones SA, Price RR, Watson MA, McKee DD, Moore LB, et al. A regulatory cascade of the nuclear receptors FXR, SHP-1, and LRH-1 represses bile acid biosynthesis. Mol Cell. 2000; 6:517–526. [PubMed: 11030332]
4. Inagaki T, Choi M, Moschetta A, Peng L, Cummins CL, McDonald JG, et al. Fibroblast growth factor 15 functions as an enterohepatic signal to regulate bile acid homeostasis. Cell Metab. 2005; 2:217–225. [PubMed: 16213224]
5. Lundasen T, Galman C, Angelin B, Rudling M. Circulating intestinal fibroblast growth factor 19 has a pronounced diurnal variation and modulates hepatic bile acid synthesis in man. J Intern Med. 2006; 260:530–536. [PubMed: 17116003]
6. Kurosu H, Choi M, Ogawa Y, Dickson AS, Goetz R, Eliseenkova AV, et al. Tissue-specific expression of betaKlotho and fibroblast growth factor (FGF) receptor isoforms determines metabolic activity of FGF19 and FGF21. J Biol Chem. 2007; 282:26687–26695. [PubMed: 17623664]
7. Dawson PA, Lan T, Rao A. Bile acid transporters. J Lipid Res. 2009; 50:2340–2357. [PubMed: 19498215]
8. Dawson PA, Hubbert M, Haywood J, Craddock AL, Zerangue N, Christian WV, et al. The heteromeric organic solute transporter alpha-beta, Ostalpha–Ostbeta, is an ileal basolateral bile acid transporter. J Biol Chem. 2005; 280:6960–6968. [PubMed: 15563450]
9. Rao A, Haywood J, Craddock AL, Belinsky MG, Kruh GD, Dawson PA. The organic solute transporter alpha–beta, Ostalpha–Ostbeta, is essential for intestinal bile acid transport and homeostasis. Proc Natl Acad Sci U S A. 2008; 105:3891–3896. [PubMed: 18292224]
10. Ballatori N, Fang F, Christian WV, Li N, Hammond CL. Ostalpha–Ostbeta is required for bile acid and conjugated steroid disposition in the intestine, kidney, and liver. Am J Physiol Gastrointest Liver Physiol. 2008; 295:G179–G186. [PubMed: 18497332]
11. Hofmann AF. Bile acid malabsorption caused by ileal resection. Arch Intern Med. 1972; 130:597–605. [PubMed: 4564853]

12. Oelkers P, Kirby LC, Heubi JE, Dawson PA. Primary bile acid malabsorption caused by mutations in the ileal sodium-dependent bile acid transporter gene (SLC10A2). J Clin Invest. 1997; 99:1880–1887. [PubMed: 9109432]
13. Jung D, Inagaki T, Gerard RD, Dawson PA, Kliewer SA, Mangelsdorf DJ, et al. FXR agonists and FGF15 reduce fecal bile acid excretion in a mouse model of bile acid malabsorption. J Lipid Res. 2007; 48:2693–2700. [PubMed: 17823457]
14. Dawson PA, Haywood J, Craddock AL, Wilson M, Tietjen M, Kluckman K, et al. Targeted deletion of the ileal bile acid transporter eliminates enterohepatic cycling of bile acids in mice. J Biol Chem. 2003; 278:33920–33927. [PubMed: 12819193]
15. Haussinger, D. Preface Dig Dis; 21st international bile acid meeting; 2011. p. 5
16. Lan T, Haywood J, Rao A, Dawson PA. Molecular mechanisms of altered bile acid homeostasis in organic solute transporter-alpha knockout mice. Dig Dis. 2011; 29:18–22. [PubMed: 21691100]
17. Potthoff MJ, Boney-Montoya J, Choi M, He T, Sunny NE, Satapati S, et al. FGF15/19 regulates hepatic glucose metabolism by inhibiting the CREB-PGC-1alpha pathway. Cell Metab. 2011; 13:729–738. [PubMed: 21641554]
18. Belinsky MG, Dawson PA, Shchaveleva I, Bain LJ, Wang R, Ling V, et al. Analysis of the in vivo functions of Mrp3. Mol Pharmacol. 2005; 68:160–168. [PubMed: 15814571]
19. Heuman DM. Quantitative estimation of the hydrophilic-hydrophobic balance of mixed bile salt solutions. J Lipid Res. 1989; 30:719–730. [PubMed: 2760545]
20. Beuling E, Kerkhof IM, Nicksa GA, Giuffrida MJ, Haywood J, aan de Kerk DJ, et al. Conditional Gata4 deletion in mice induces bile acid absorption in the proximal small intestine. Gut. 2010; 59:888–895. [PubMed: 20581237]
21. Williams DL, Newman TC, Shelness GS, Gordon DA. Measurement of apolipoprotein mRNA by DNA-excess solution hybridization with single-stranded probes. Methods Enzymol. 1986; 128:671–689. [PubMed: 3755211]
22. Timmins JM, Lee JY, Boudyguina E, Kluckman KD, Brunham LR, Mulya A, et al. Targeted inactivation of hepatic Abca1 causes profound hypoalpha-lipoproteinemia and kidney hypercatabolism of apoA-I. J Clin Invest. 2005; 115:1333–1342. [PubMed: 15841208]
23. Wang DQ, Tazuma S, Cohen DE, Carey MC. Feeding natural hydrophilic bile acids inhibits intestinal cholesterol absorption: studies in the gallstone-susceptible mouse. Am J Physiol Gastrointest Liver Physiol. 2003; 285:G494–G502. [PubMed: 12748061]
24. Lambert G, Amar MJ, Guo G, Brewer HB Jr, Gonzalez FJ, Sinal CJ. The farnesoid X-receptor is an essential regulator of cholesterol homeostasis. J Biol Chem. 2003; 278:2563–2570. [PubMed: 12421815]
25. Kim I, Ahn SH, Inagaki T, Choi M, Ito S, Guo GL, et al. Differential regulation of bile acid homeostasis by the farnesoid X receptor in liver and intestine. J Lipid Res. 2007; 48:2664–2672. [PubMed: 17720959]
26. Li-Hawkins J, Gafvels M, Olin M, Lund EG, Andersson U, Schuster G, et al. Cholic acid mediates negative feedback regulation of bile acid synthesis in mice. J Clin Invest. 2002; 110:1191–1200. [PubMed: 12393855]
27. Balistreri WF, Heubi JE, Suchy FJ. Bile acid metabolism: relationship of bile acid malabsorption and diarrhea. J Pediatr Gastroenterol Nutr. 1983; 2:105–121. [PubMed: 6350555]
28. Weis HJ, Dietschy JM. Adaptive responses in hepatic and intestinal cholesterogenesis following ileal resection in the rat. Eur J Clin Invest. 1974; 4:33–41. [PubMed: 4819833]
29. Akerlund JE, Reihner E, Angelin B, Rudling M, Ewerth S, Bjorkhem I, et al. Hepatic metabolism of cholesterol in Crohn's disease. Effect of partial resection of ileum Gastroenterology. 1991; 100:1046–1053.
30. Soroka CJ, Velazquez H, Mennone A, Ballatori N, Boyer JL. Ostalpha depletion protects liver from oral bile acid load. Am J Physiol Gastrointest Liver Physiol. 2011; 301:G574–G579. [PubMed: 21719738]
31. Sinha J, Chen F, Miloh T, Burns RC, Yu Z, Shneider BL. Beta-Klotho and FGF-15/19 inhibit the apical sodium-dependent bile acid transporter in enterocytes and cholangiocytes. Am J Physiol Gastrointest Liver Physiol. 2008; 295:G996–G1003. [PubMed: 18772362]

32. Walters JR, Tasleem AM, Omer OS, Brydon WG, Dew T, le Roux CW. A new mechanism for bile acid diarrhea: defective feedback inhibition of bile acid biosynthesis. Clin Gastroenterol Hepatol. 2009; 7:1189–1194. [PubMed: 19426836]

33. Vlahcevic ZR, Bell CC Jr, Buhac I, Farrar JT, Swell L. Diminished bile acid pool size in patients with gallstones. Gastroenterology. 1970; 59:165–173. [PubMed: 4915192]

Abbreviations

BA	bile acid(s)
Asbt	apical sodium-dependent bile acid transporter
Ost	organic solute transporter
FXR	farnesoid X receptor
FGF15	fibroblast growth factor 15
Cyp7a1	cholesterol 7α-hydroxylase
FGFR4	fibroblast growth factor receptor 4
CA	cholic acid
WT	wild type
HRP	horse radish peroxidase
DKO	double knockout
BW	body weight
TC	taurocholate
TβMC	tauro-β-muricholate
CE	cholesteryl ester
ER	endoplasmic reticulum
HMGCR	HMG CoA reductase
HMGCS1	HMG CoA synthase

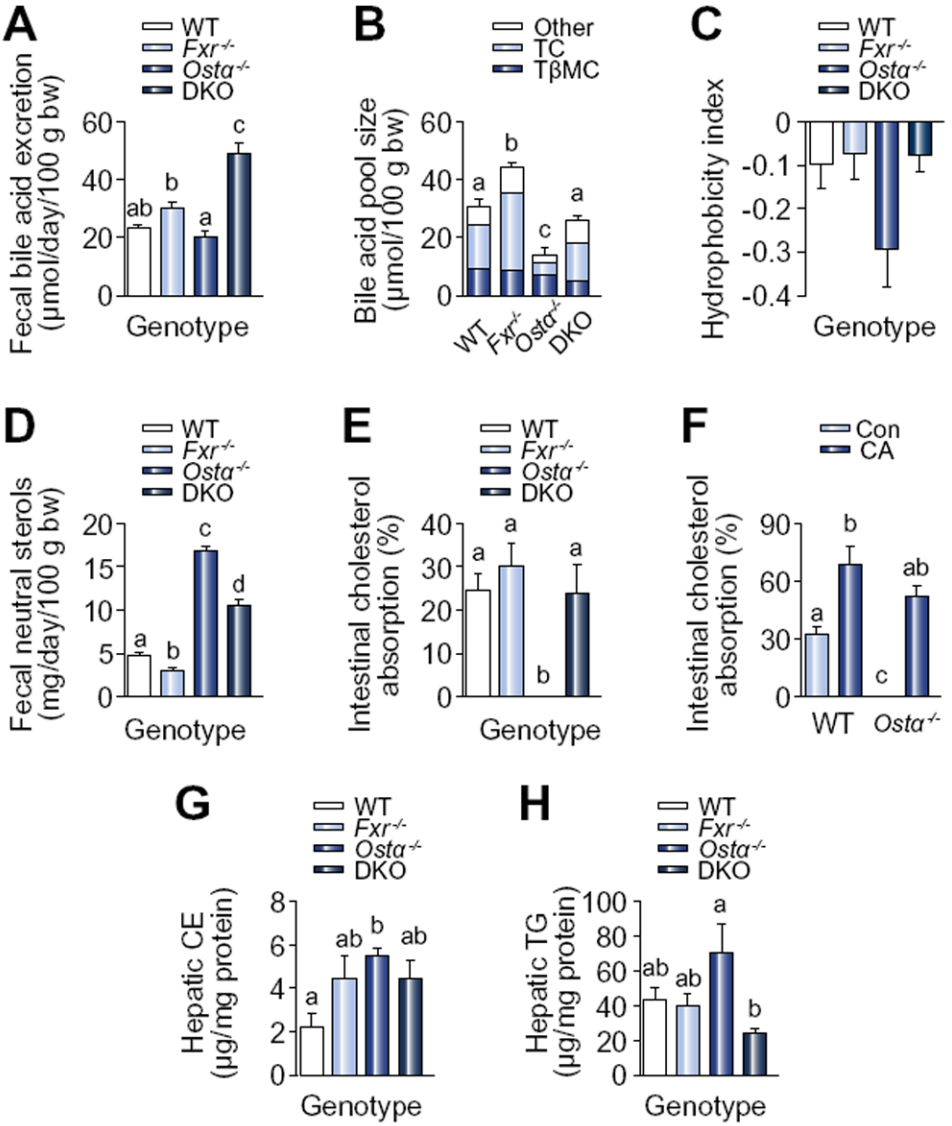

Fig. 1. BA metabolism, intestinal cholesterol absorption, and hepatic lipids

Male mice were analyzed. (A) Fecal BA excretion (n = 10). (B) BA pool size and composition (n = 5). (C) Calculated hydrophobicity index of the BA pool (n = 5). (D) Fecal neutral sterol excretion (n = 10). (E) Intestinal cholesterol absorption (n = 5). (F) WT and *Osta*$^{-/-}$ mice (3–5 months of age) were fed a control diet or a diet containing 0.2% CA for 7 days prior to measuring intestinal cholesterol absorption (n = 3–4). (G) Hepatic cholesteryl ester content (n = 5). (H) Hepatic triglyceride content (n = 5). Different lowercase letters indicate significant differences (p <0.05) between groups. DKO, *Osta*$^{-/-}$/*Fxr*$^{-/-}$ double knockout; TC, taurocholate; TβMC, tauro-β-muricholate; Con, control diet; CA, 0.2% CA-containing diet. CE, cholesteryl ester.

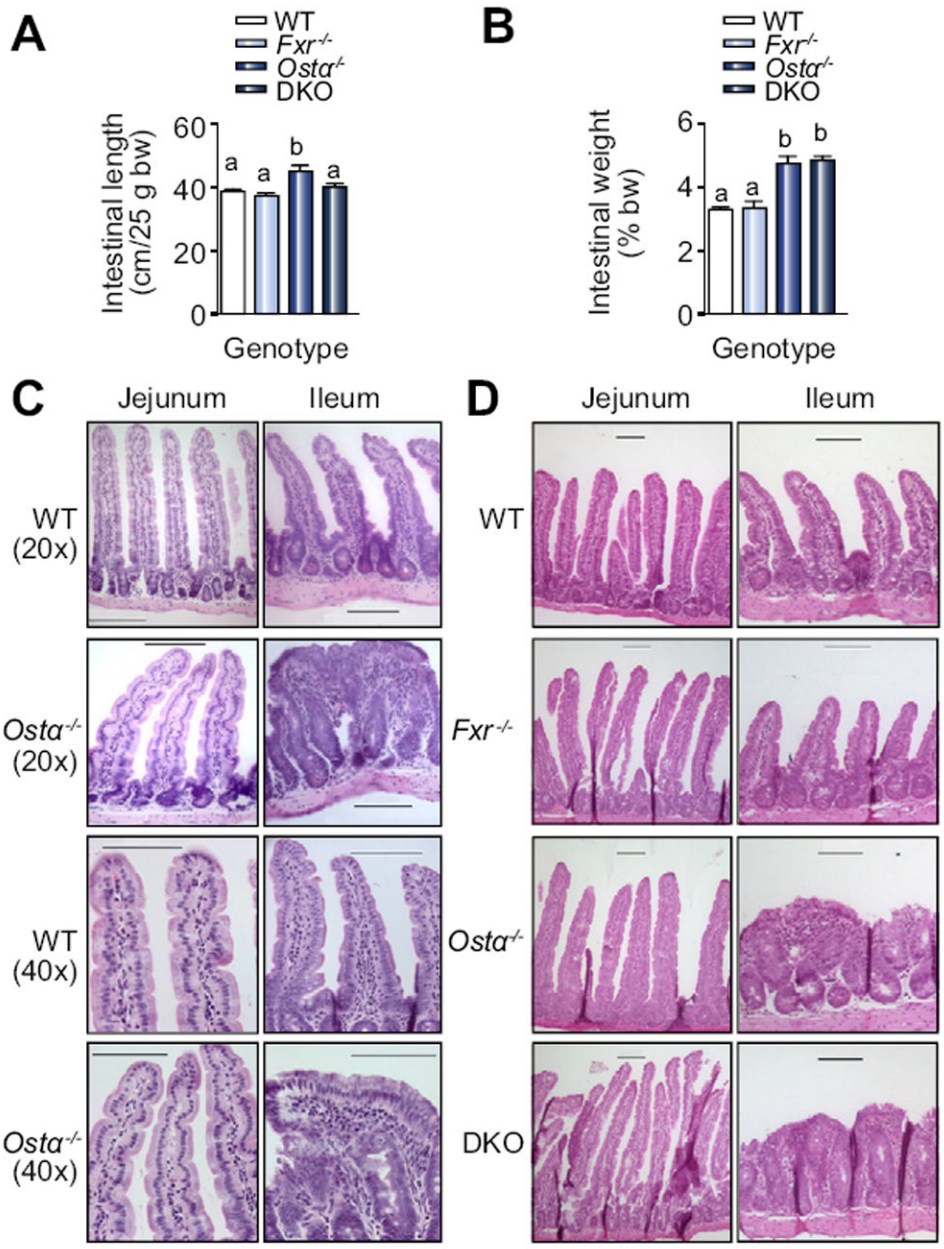

Fig. 2. Intestinal length, weight, and villus morphology

(A) Length and (B) weight of the small intestine was measured in male mice (n = 10). (C) Representative light micrographs of hematoxylin-eosin-stained transverse sections of jejunum and ileum from WT and *Osta*$^{-/-}$ mice. (D) Representative light micrographs of hematoxylin-eosin-stained transverse sections of jejunum and ileum from the indicated genotypes. Images are shown at 20× magnification. Black bar, 100 μm.

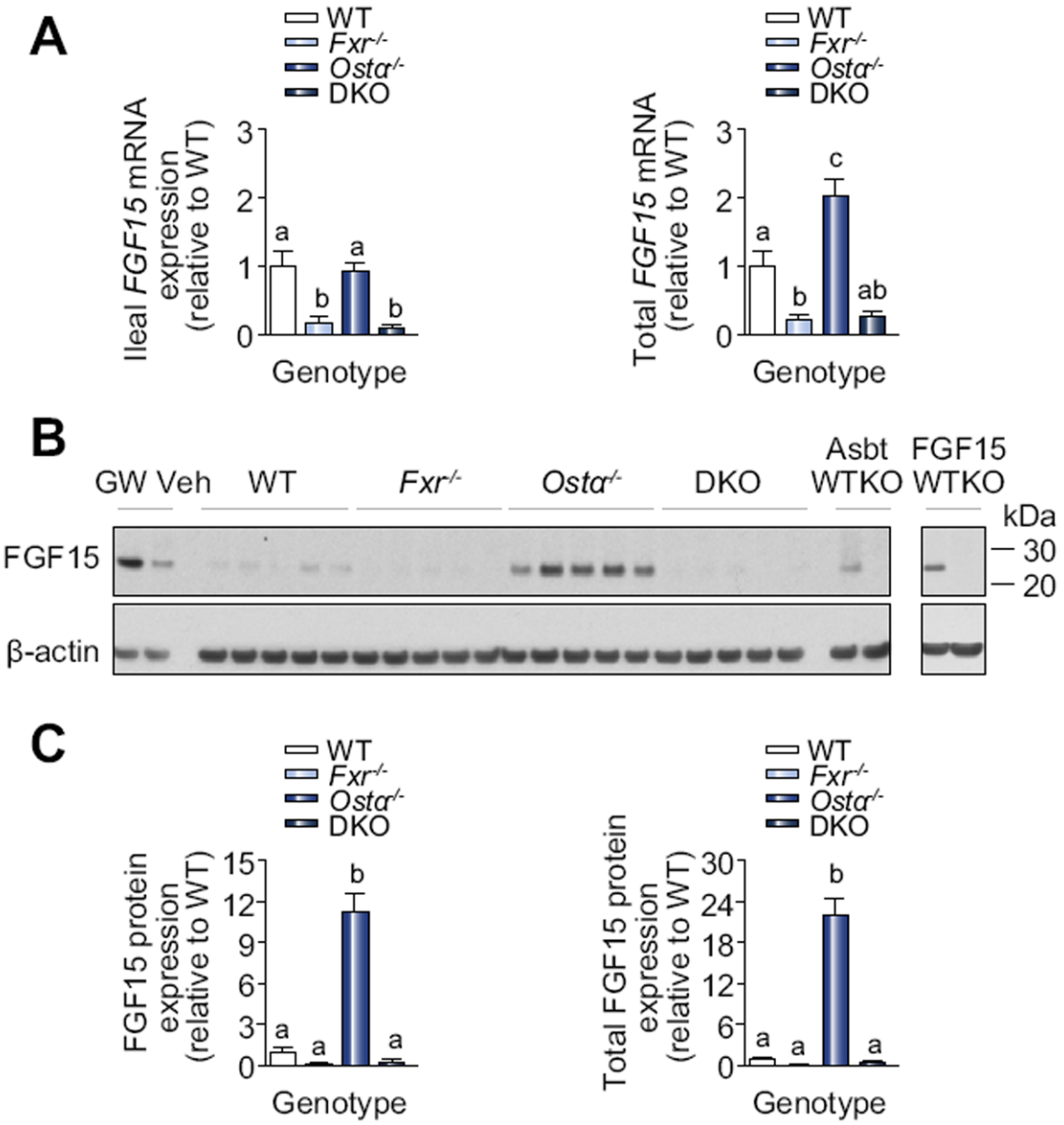

Fig. 3. Ileal FGF15 expression

Male mice were analyzed (n = 5). (A) Ileal *FGF15* mRNA expression. Total ileal *FGF15* mRNA expression was calculated by normalizing the mRNA expression determined by real time PCR to the total RNA yield from ileum for each animal. (B) Ileal FGF15 protein expression in individual mice from the indicated genotypes. As a control, ileal extracts from WT mice treated with vehicle or GW4064 (n = 2–4; pooled) and from WT, $Asbt^{-/-}$ (n = 5; pooled), and $Fgf15^{-/-}$ mice (n = 6; pooled) were also analyzed. (C) Ileal FGF15 protein expression was quantified by densitometry. Values for individual mice were normalized to β-actin expression and are expressed relative to WT mice. Total ileal FGF15 protein expression was calculated by normalizing the protein expression determined by immunoblotting to total protein yield from ileum for each animal. Different lowercase letters indicate significant differences ($p < 0.05$) between groups.

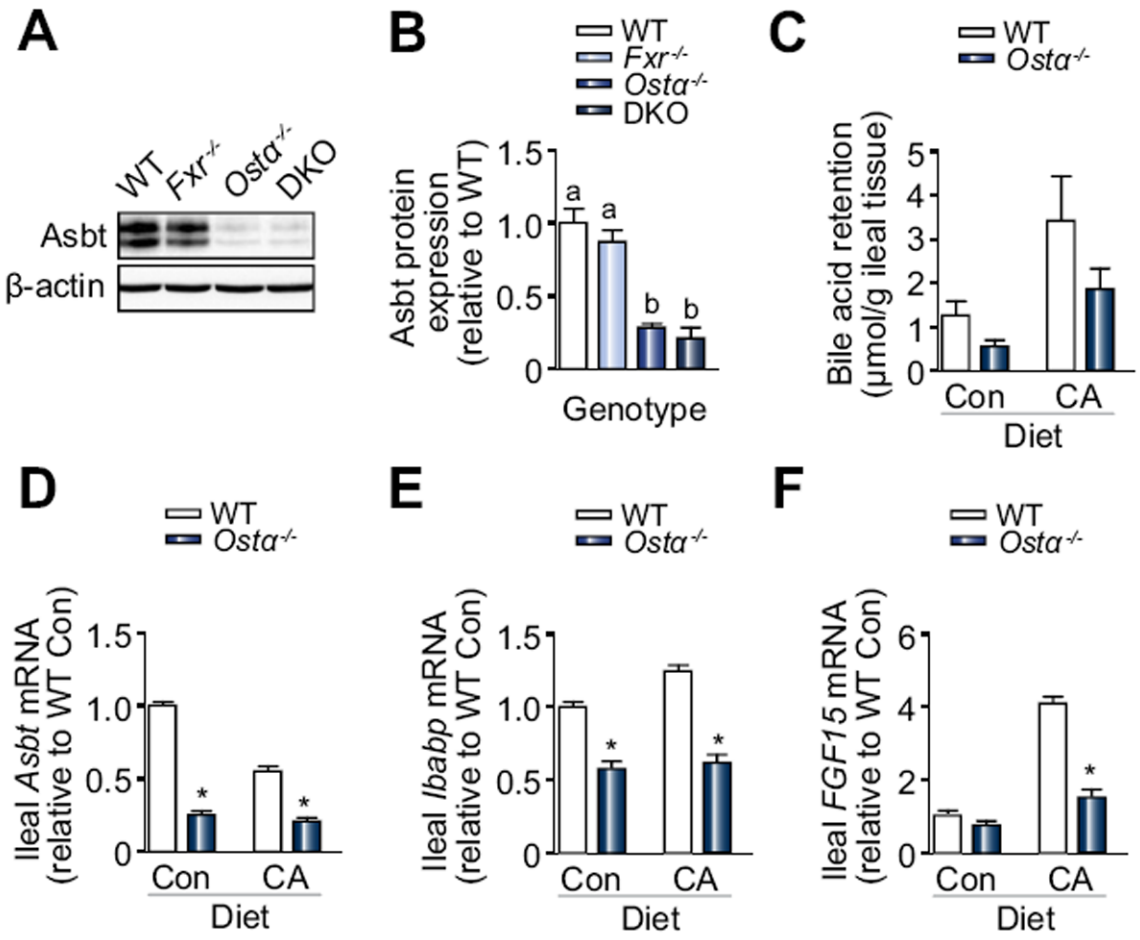

Fig. 4. Ileal gene expression and BA accumulation

RNAs and proteins were isolated from ileum (segment 5) of individual male mice (n = 5) and used for real-time PCR analysis and immunoblotting. (A) Protein extracts from individual mice were pooled (50 μg) and subjected to immunoblotting. (B) Ileal Asbt protein expression was analyzed in individual mice. Values are expressed relative to WT mice. Different lowercase letters indicate significant differences (p <0.05) between groups. (C) Measurement of ileal tissue-associated BA in WT and *Osta*$^{-/-}$ mice fed a control diet or a diet containing 0.2% CA for 4.5 days. Ileal mRNA expression of (D) *Asbt*, (E) *Ibabp*, and (F) *FGF15*. An asterisk indicates significant differences (p <0.05) as compared to WT mice for that diet group.

Table 1

Hepatic gene expression (relative to WT).

Gene	Genotype			
	Fxr$^{-/-}$	*Ostα*$^{-/-}$	DKO	*Ostα*$^{-/-}$/WT
ABCA1	0.98 ± 0.03	0.79 ± 0.03 *	0.94 ± 0.06	↓
ABCG5	0.77 ± 0.02	1.04 ± 0.08	0.94 ± 0.17	↔
ASBT	0.91 ± 0.22	1.14 ± 0.13	0.82 ± 0.20	↔
BSEP	0.61 ± 0.06 *	0.92 ± 0.03	0.74 ± 0.04 *	↔
CYP7A1	1.43 ± 0.28	0.26 ± 0.07 *	2.01 ± 0.33 *	↓
CYP8B1	1.93 ± 0.18 *	0.72 ± 0.12	2.96 ± 0.36 *	↔
CYP27A1	0.92 ± 0.60	0.96 ± 0.13	0.93 ± 0.03	↔
FGFR4	1.04 ± 0.07	0.80 ± 0.07	1.35 ± 0.12 *	↔
FXRα	n.d.	1.11 ± 0.05	n.d.	↔
FXRα1,2	n.d.	0.84 ± 0.03	n.d.	↔
FXRα3,4	n.d.	1.39 ± 0.08 *	n.d.	↑
HMGCR	0.83 ± 0.13	0.87 ± 0.10	1.86 ± 0.29 *	↔
HMGCS1	1.44 ± 0.23	1.69 ± 0.37	4.25 ± 0.77 *	↔
HNF4α	0.84 ± 0.06	0.79 ± 0.06	0.74 ± 0.05 *	↔
MRP2	0.96 ± 0.13	0.49 ± 0.05 *	0.50 ± 0.11 *	↓
MRP3	0.97 ± 0.19	0.91 ± 0.08	0.98 ± 0.08	↔
MRP4	1.49 ± 0.12 *	0.95 ± 0.13	2.75 ± 0.12 *	↔
NTCP	0.77 ± 0.03 *	1.07 ± 0.06	1.04 ± 0.05	↔
PXR	0.69 ± 0.06 *	1.07 ± 0.17	0.64 ± 0.07 *	↔
SR-BI	0.64 ± 0.03 *	0.63 ± 0.04 *	0.40 ± 0.04 *	↓
SHP	0.69 ± 0.16	0.78 ± 0.07	0.47 ± 0.12	↔

Data are shown ± SEM (n = 5 mice per group).

* Significant changes (p <0.05) *vs.* WT.

Arrows indicate the direction of changes in *Ostα*$^{-/-}$ mice *vs.* WT. n.d., not determined.

Table 2

Ileal gene expression (relative to WT).

Gene	Genotype			
	Fxr$^{-/-}$	*Ostα*$^{-/-}$	DKO	*Ostα*$^{-/-}$/WT
ABCA1	1.66 ± 0.27	0.40 ± 0.06*	0.45 ± 0.02*	↓
ABCG5	1.26 ± 0.24	0.44 ± 0.07*	0.65 ± 0.16	↓
ASBT	0.90 ± 0.15	0.74 ± 0.10	0.64 ± 0.13*	↔
FGF15	0.19 ± 0.07*	0.93 ± 0.14	0.12 ± 0.03*	↔
FGFR4	1.11 ± 0.08	2.11 ± 0.23*	2.53 ± 0.35*	↑
FXRα	n.d.	0.66 ± 0.06*	n.d.	↓
FXRα1,2	n.d.	0.64 ± 0.07*	n.d.	↓
FXRα3,4	n.d.	0.72 ± 0.05*	n.d.	↓
HMGCR	1.08 ± 0.11	1.34 ± 0.06*	1.33 ± 0.20	↑
HMGCS1	1.10 ± 0.13	1.13 ± 0.09	1.31 ± 0.32	↔
HNF1α	1.14 ± 0.10	1.03 ± 0.11	0.96 ± 0.09	↔
HNF4α	0.93 ± 0.09	0.68 ± 0.02*	0.62 ± 0.08*	↓
IBABP	0.03 ± 0.01*	0.91 ± 0.12	0.07 ± 0.01*	↔
MRP3	1.12 ± 0.14	0.96 ± 0.08	0.83 ± 0.03	↔
MRP4	1.16 ± 0.14	1.31 ± 0.06*	1.04 ± 0.07	↑
NPC1L1	1.01 ± 0.18	0.34 ± 0.08*	0.43 ± 0.09*	↓
Ostβ	0.40 ± 0.05*	0.50 ± 0.03*	0.21 ± 0.02*	↓
PXR	0.86 ± 0.09	0.72 ± 0.06*	0.80 ± 0.07*	↓
SHP	0.13 ± 0.08	0.20 ± 0.07	0.17 ± 0.11	↔
SLC13A1	0.67 ± 0.03*	0.29 ± 0.06*	0.29 ± 0.05*	↓

Data are shown ± SEM (n = 5 mice per group).

* Significant changes (p <0.05) *vs.* WT.

Arrows indicate the direction of changes in *Ostα*$^{-/-}$ mice *vs.* WT.

Table 3

Phenotypic changes in *Fxr*$^{-/-}$, *Osta*$^{-/-}$ and *Osta*$^{-/-}$/*Fxr*$^{-/-}$ mice (relative to WT).

	Genotype		
Parameter	***Fxr*$^{-/-}$**	***Osta*$^{-/-}$**	**DKO**
Morphology			
Small intestinal length	↔	↑	↔
Small intestinal weight	↔	↑	↑
Ileal weight	↔	↑↑	↑↑
Ileal DNA content	↔	↑↑	↑↑
Ileal RNA content	↔	↑↑	↑↑
Ileal villus height	↔	↓↓	↓↓
Ileal villus width	↔	↑↑	↑↑
Ileal crypt depth	↑	↑↑	↑↑
BA and chol metabolism			
BA excretion	↑	↔	↑↑
BA pool size	↑↑	↓↓	↔
Plasma BA	↑	↔	↑
Hydrophobicity index	↔	↓↓	↔
Total plasma chol	↑	↔	↔
Hepatic CE	↔	↑	↔
Hepatic Cyp7a1	↑	↓	↑
Hepatic Cyp8b1	↑	↓	↑↑
Ileal FGF15 protein	↓	↑↑	↓

Arrows indicate the direction of changes *vs.* WT mice.